

Weighing the cusp at the Galactic Centre

N. M¹, A. E¹, S. P¹, R. S¹, J. M¹, and R. S²

¹ I. Physikalisches Institut, Universität zu Köln, Zùlpicher Str.77, 50937 Köln, Germany

² Astronomisches Recheninstitut, Mönchhofstr. 12-14, 69120 Heidelberg, Germany

Received <date>; accepted <date>; published online <date>

Abstract. As stars close to the galactic centre have short orbital periods it has been possible to trace large fractions of their orbits in the recent years. Previously the data of the orbit of the star S2 have been fitted with Keplerian orbits corresponding to a massive black hole (MBH) with a mass of $M_{BH}=3-4\times 10^6 M_{\odot}$ implying an insignificant cusp mass. However, it has also been shown that the central black hole resides in a $\sim 1''$ diameter stellar cluster of a priori unknown mass. In a spherical potential which is neither Keplerian nor harmonic, orbits will precess resulting in inclined rosetta shaped trajectories on the sky. In this case, the assumption of non-Keplerian orbits is a more physical approach. It is also the only approach through which cusp mass information can be obtained via stellar dynamics of the cusp members. This paper presents the first exemplary modelling efforts in this direction. Using positional and radial data of star S2, we find that there could exist an unobserved extended mass component of several $10^5 M_{\odot}$ forming a so-called ‘cusp’ centered on the black hole position. Considering only the fraction of the cusp mass $M_{S2_{apo}}$ within the apo-center of the S2 orbit we find as an upper limit that $M_{S2_{apo}}/(M_{BH} + M_{S2_{apo}}) \leq 0.05$. A large extended cusp mass, if present, is unlikely to be composed of sub-solar mass constituents, but could be explained rather well by a cluster of high M/L stellar remnants, which we find to form a stable configuration.

Key words: Galactic Centre – Stellar dynamics – Stellar cluster – Cusp – Black Hole

©0000 WILEY-VCH Verlag GmbH & Co. KGaA, Weinheim

1. Introduction

Over the last decade, evidence has been found for the existence of massive black holes (MBH) in the centres of many nearby galaxies. With increasing observational data – 12 MBHs candidates detected until 1995 (Kormendy & Richstone 1995), and more than 37 until 2001 (Kormendy 2001, Ferrarese et al. 2001) – it is argued that most galaxies harbor nuclei dominated by MBHs with masses that range between 10^6 and $10^{9.5}$ solar masses.

Located at a distance of only ~ 8 kpc from the solar system (Reid 1993; Eisenhauer 2003), the Galactic Centre (GC) is the closest and therefore best object for investigating physical processes in the galactic nucleus of a typical spiral galaxy. It offers a unique “laboratory” for studying stars and gas in the sphere of influence on a super-massive black hole, (e.g., Genzel, Hollenbach, & Townes 1994; Morris & Serabyn 1996; Mezger, Duschl, & Zylka 1996; Melia & Falcke 2001), with a degree of detail that cannot be accessed in any other galactic nucleus in the foreseeable future. With the now available high sensitivity and angular resolution,

large ground-based telescopes offer the opportunity to obtain an unprecedented view of the Galactic centre. Initially, with speckle imaging techniques and lately with adaptive optics techniques, high angular resolution images on the Galaxy’s central cluster were obtained. This first set of observations was able to measure stellar motions on the plane of the sky, yielding estimates of the projected velocities (Eckart & Genzel 1996; Ghez et al. 1998), projected accelerations (Ghez et al. 2000; Eckart et al. 2002a), and three-dimensional orbital motions (Eckart et al. 2002a, Schödel et al. 2002, 2003; Ghez et al. 2003b), which each provided a successively stronger case for a super-massive black hole at the centre of the Milky Way and its association with the unusual radio source Sgr A* (Lo et al. 1985).

More than a decade of high-resolution infrared observations of proper motions in the GC, with the ESO New Technology Telescope (NTT) and the ESO Very Large Telescope (VLT) (Eckart & Genzel 1996; Eckart et al. 2002a; Schödel et al. 2002, 2003), as well as with the Keck telescope (Ghez et al. 1998, 2000, 2003b), have revealed at least 6 stars that show substantial acceleration due to the super-massive black hole associated with Sgr A* and are on bound orbits around it. With a peri-centre of less than 0.6 mpc (15 mas) and an

orbital period of ~ 15 years, S2 is the most striking case of these.

A series of observations with the NAOS/CONICA adaptive optics system/near-infrared camera at the ESO VLT unit telescope 4 that covered the peri-centre passage of the star S2 around Sgr A* allowed Schödel et al. (2002) to approximate a Keplerian orbit and to measure the enclosed dark mass down to a distance of ~ 0.6 mpc from Sgr A*. With these observations, they could exclude a neutrino ball scenario (Munyanza & Viollier, 2002) as an alternative explanation for the dark mass concentration. They excluded as well a cluster of dark astrophysical objects (Maoz 1998) such as neutron stars, leaving a central super-massive black hole as the most probable explanation.

Using the Keck 10m telescope, Ghez et al. (2003a) measured a Keplerian orbit for the star S2 which agreed with the results of Schödel et al. (2002). Additionally, Ghez et al. (2003a) reported the first detection of spectral absorption lines (both Br γ (2.1661 μm) and He I (2.1126 μm)), providing the first line-of-sight velocity measurements of star S2. These measurements resolved the ambiguity on the inclination of the S2 orbit indicating that its position was behind the black hole when it passed through its peri-centre. In addition, stellar rotational velocities suggest that S2 is an O8-B0 dwarf star and thus a massive ($\sim 15 M_{\odot}$) young star (≤ 10 Myrs).

From data taken with NAOS/CONICA and the new NIR integral field spectrometer SPIFFI at the ESO VLT, Eisenhauer et al. (2003) reported new astrometric observations and additional spectroscopic observations of the star S2, reducing the uncertainties on the orbital parameters. They also gave the most accurate primary distance measurement to the centre of the Milky Way of 7.94 ± 0.42 kpc, which is in agreement with earlier determinations (see Reid 1993).

In this paper, we explore the possibility that there exists a compact, continuous mass distribution composed of several undetectable faint stars or perhaps some more exotic material in addition to the point mass of Sgr A*. In this case, the orbit of S2 will not follow a simple Keplerian orbit, but will rather show peri-centre-shifts that result in rosetta shaped orbits. This idea is motivated by the observation that the stellar density does not flatten out, but exhibits a steep peak towards the centre, a so-called cusp (Eckart et. al, 1995; Alexander, 1999; Genzel et al., 2003). In contrast to earlier studies, the main approach of this work is that the mass-to-light ratio, M/L , is *not* considered to be constant over the entire range of the GC stellar cluster. Indeed, there are indications that the stellar population varies with position and is not quite well mixed (Alexander, 1999). Furthermore, the exact composition of the cusp is still unknown and our current understanding of the stellar distribution in the GC is incomplete (Genzel et al. 2003). With current observations, low-mass stars ($K \geq 21$ mag) cannot be observed in these dense cusp regions and the true value of the M/L ratio is not known. Also, as pointed out by Baumgardt et al. (2003), dynamical evolution of a dense stellar cluster will result in a strong increase of M/L ratio by segregation of stellar evolution remnants to the centre. On the other hand, the approximation that the dynamics in the central region is Keplerian is directly related to the implicit

assumption of Eckart et al. (2002a), Schödel et al. (2002), and Ghez et al. (2003a) that the M/L ratio at 2 μm in the cusp is as low as in the outer stellar cluster ($M/L = 2M_{\odot}/L_{\odot}$).

Considering these circumstances, stars with short orbital periods, in particular the star S2, of which orbital data are best known, play a key role in exploring the gravitational potential. We show that the present observational data on S2 cannot discriminate between a *Keplerian* and a *non-Keplerian* potential. Subsequently, we study the influence of an extended distribution of dark mass near Sgr A* taking into consideration the constraints set by the orbit of S2 as well as the limits set on the total enclosed mass at larger radii. In this study relativistic effects are neglected as they are second order corrections.

In § 2 we outline our modelling of the density distribution of the central region and show that the star counts near Sgr A* can be described by a compact Plummer model core. The method used to compute orbits in non-Keplerian potentials is explained in § 3. In § 4 possible orbital models for S2 are presented. We discuss the implications of the limits on the cusp mass derived from the *non-Keplerian* orbit modelling in § 5, and draw our conclusions in § 6.

2. Modelling the stellar cluster and the enclosed mass

In this section it is described how the most recent observations of the GC star cluster (Genzel et al., 2000, 2003) can be used to model the mass distribution function as close as a few milli-parsecs from Sgr A*. A surface density profile is fitted to number density counts and used, together with dynamical mass estimators, to deduce the 3 dimensional mass distribution function. By following this approach, we have assumed that the visible stars trace the mass distribution of the cluster.

2.1. Density model of the stellar cluster

Genzel et al. (2003, see their Fig.7) determined the surface number density of stars in the central parsec by counting the sources in annuli with increasing radius around Sgr A*. Within ~ 2 arc-seconds of Sgr A*, their data indicate an excess of faint stars above the counts expected in a cluster with a flat core, as it had been already suggested earlier (Eckart et al. 1995; Alexander 1999). They confirmed the existence of a "cusp" and showed that it is centred at a position of ($\Delta \alpha$, $\Delta \delta$) = (+0.09", -0.15") from Sgr A*, with an uncertainty of ± 0.2 ". Here we use the same K-band counts ($K \leq 18$) together with the earlier SHARP/NTT counts ($K \leq 15$), without taking into our study their higher magnitude limit H-band counts ($H \leq 19$). In contrast to the 'by-eye' H-band counts, the K-band counts, were determined by an automated procedure, they are therefore possibly less biased, and cover the whole range of the cluster, not only the central arc-second.

Genzel et al. (2003) fitted a broken power-law to their stellar counts, with a distinct break at 10 arcsec. In this section, we show that it is also possible to fit the number density counts with a superposition of several Plummer models. The

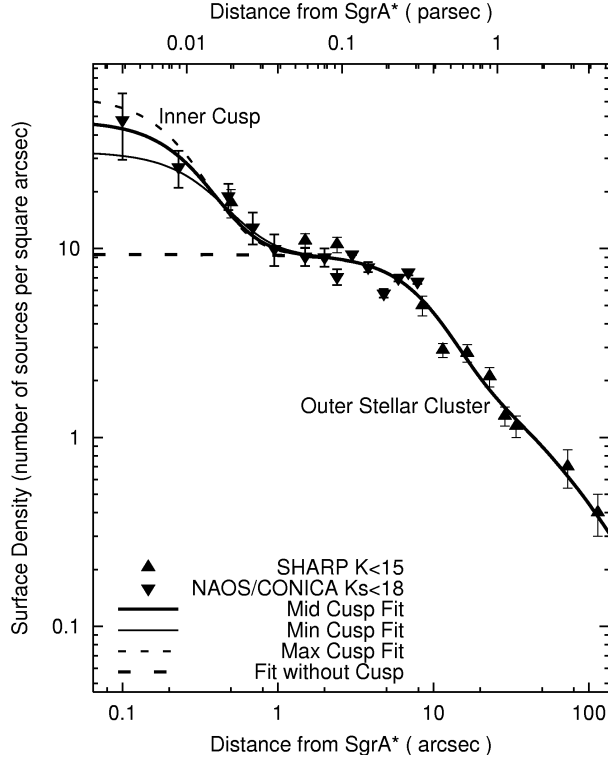


Fig. 1. Surface density of stars vs. distance from Sgr A*. The downward pointing triangles represent the CONICA/NAOS data for $K_s \leq 18$, the upward pointing triangles are SHARP/NTT data for $K_s \leq 15$ stars scaled up by a factor of 5 in order to match the fainter NAOS/CONICA counts. The data are taken from Genzel et al. (2000, 2003). The long-dashed line is the superposition of the 5 outermost Plummer models (see, Table 1). The addition of the innermost Plummer model (the 'inner' cusp) gives the 'composite model'. It is represented by the 3 other curves, where the thick-straight line corresponds to the middle values of the 'inner cusp' parameters R_1 and M_1 , the thin-straight line to its lower values, and the short-dashed line to its upper values. and the short-dashed line to its upper values.

Plummer model has the advantage of being analytically integrable. It resembles actual clusters with compact cores and an extended outer envelope (Spitzer 1975).

In this model the 3 dimensional radial density distribution $\rho(r)$ and the projected mass density $\sigma(r)$ are described by:

$$\rho(r) = \frac{3M}{4\pi R^3} \frac{1}{\left(1 + \frac{r^2}{R^2}\right)^{\frac{5}{2}}}, \quad (1)$$

$$\sigma(r) = \frac{4\rho(0)R}{3} \frac{1}{\left(1 + \frac{r^2}{R^2}\right)^2}, \quad (2)$$

where R is the core radius and M the total mass.

Our best surface density fit to the data consists of a superposition of 6 different Plummer models, which will be termed in the following as 'composite model':

$$\sigma(r) = \sum_{i=1}^6 \frac{M_i}{\pi} \frac{R_i^2}{(r^2 + R_i^2)^2}. \quad (3)$$

The six values of the core radii, R_i , are given in Table 1. Fits with larger numbers of Plummer models are possible as

Table 1. The parameters of the 'composite model' used to fit the GC stellar cluster. For each Plummer model we give the value of the core radius R_i (in arcsec and in parsec) deduced from the surface density plot. M_i is the corresponding total mass scaled to the enclosed mass distribution (Fig. 2). M_{apo_i} is the contribution in mass inside a sphere which has a radius equal to the apo-astron of S2. ρ_i is the calculated average density in $M_\odot \cdot \text{pc}^{-3}$. The first Plummer model ($R_1 = 0.4''$ or 0.015 pc) corresponds to the inner cusp centered at Sgr A*. The addition of the remaining 5 models represents the density distribution of the outer stellar cluster.

i	R_i [arcsec]	R_i [pc]	M_i [M_\odot]	M_{apo_i} [M_\odot]	$\rho_i(0)$
1	0.4	0.015	8540	1080	6.0×10^8
2	13	0.5	1.8×10^6	10	3.5×10^6
3	52	2.0	2.7×10^6	0.25	7.9×10^4
4	97	3.8	6.7×10^6	0.01	2.9×10^4
5	220	8.5	13.1×10^6	0.002	5.1×10^3
6	321	12.4	27.6×10^6	0.001	3.4×10^3

well; six was the smallest numbers of components with which we were able to represent the data, i.e. the cusp plus the stellar cluster.

2.2. The enclosed mass

Similarly to eq.3, the mass distribution of the 'composite model' is given by

$$M(r) = \sum_{i=1}^6 \frac{M_i r^3}{(r^2 + R_i^2)^{3/2}}. \quad (4)$$

Under the assumption that the visible stars trace the mass, the M_i can be determined by fitting eq.4 to the dynamical enclosed mass estimates.

In order to calibrate the enclosed mass $M(r)$ we only rely on a solid measure of the central mass (within 0.001 pc from SgrA*) derived from the Keplerian orbit of the star S2 and mass estimates of the entire stellar cluster at distances of several parsecs from the center. At these large radii the published results of all different statistical mass estimators give very consistent results within uncertainties that are fully acceptable for our study (Eisenhauer 2003, Genzel et al. 2000, Serabyn & Lacy 1985; Güsten et al. 1987; Lacy et al. 1991; Herbst et al. 1993; Roberts & Goss 1993). By tying our mass modelling as a function of radius to the stellar number density distribution, it does not depend on possible anisotropies of the velocity field at radii of less than a parsec. It is only there where the anisotropies are apparently present at a considerable level (Genzel et al. 2000, Schödel et al. 2003). In particular we would like to point out that we are not fitting to enclosed mass estimates at these small radii. In Fig.2 these are only shown for completeness. The only assumption that goes into our considerations is that of a constant M/L ratio as a function of distance. This assumption is relaxed and discussed in the following sections of the paper.

Our best fit to these dynamical mass estimates corresponds to a $2.9 \times 10^6 M_\odot \pm 0.3 \times 10^6 M_\odot$ black hole plus the

mass distribution of eq.4, of which the 6 total masses M_i , are listed together with their corresponding densities, ρ_i , in Table 1. An offset in the value of the enclosed compact mass will not influence our modelling significantly because the shape and mass of our cluster composite model depends primarily on the profile of the stellar number counts.

The combination of the five outermost components gives a similar configuration as the flattened isothermal sphere of core radius ~ 0.3 pc derived by Genzel et al. (2003) (see mass densities below). Fig. 1 shows that there exists a mini-core centered on Sgr A*, which we denominate by the 'inner cusp'. It is represented by the innermost Plummer model with a core radius $R_1 = 15.5 \text{ mpc} \cong 0.4''$.

With an apo-centre of approximately 9 mpc (Schödel, 2004; Ghez et al., 2003a), the star S2 orbits in a region inside the core radius ($R_1 \sim 15 \text{ mpc}$) of this innermost model. Therefore its path can be mainly influenced, in addition to the BH potential, by the 'inner cusp' gravitational potential (see column 5 in Table 1). At these distances from the centre, the present number density counts have large error bars (see Fig. 1). The limits on the core radius, R_1 , of our model, deduced from the error bars on the number density counts, are found to be 13.2 mpc for the lower value R_1^{min} , and 20.2 mpc for the upper one R_1^{max} . Varying the mass, M_1 , of the central Plummer model component allows to study cases in which the mass-to-light ratio, M/L , varies as a function of distance from Sgr A*. As described in § 3 and § 4, exploring the possible ranges for R_1 and M_1 that fulfill the constraints given by the orbital measurements of star S2 allows to derive dynamical information on the cusp mass. In the following, we make use of this model which fixes the density profile of the cusp to the stellar profile.

In Fig. 2 the long-dashed line corresponds to our best fit, the thick-straight line shows only the enclosed mass without a BH obtained with our model of the extended cluster. The thin-straight and the short-dashed lines represent the above discussed extreme cases of an inner cusp radius $R_1 = R_1^{\text{min}} = 13.2$ mpc with $M = 8540 M_\odot$ and $R_1 = R_1^{\text{max}} = 20.2$ mpc with $M = 8820 M_\odot$. Note that these errors result from the uncertainties of the stellar number counts at the smallest distances to Sgr A* (Fig. 1).

The density of the 'inner cusp' is a few hundred times larger than that of the second Plummer model and it has a ~ 33 times smaller core radius (see Fig. 1 and Table 1). Our model implies density values as high as $1.68 \times 10^8 M_\odot \text{pc}^{-3}$ at $0.1''$, and $1.54 \times 10^7 M_\odot \text{pc}^{-3}$ at $1''$. These values are comparable to the ones derived by Genzel et al. (2003) from a broken power-law density profile ($7 \times 10^8 M_\odot \text{pc}^{-3}$ at $0.1''$ and $3 \times 10^7 M_\odot \text{pc}^{-3}$ at $1''$).

In the following we will use the above derived mass distribution to determine the path of S2 in response to this non-point mass potential plus the central black hole.

3. Modelling the orbit of S2

In order to fit non-Keplerian orbits to the measured time-dependent positions of the star S2 in the above described type of mass potential, one needs a high accuracy integrator. For

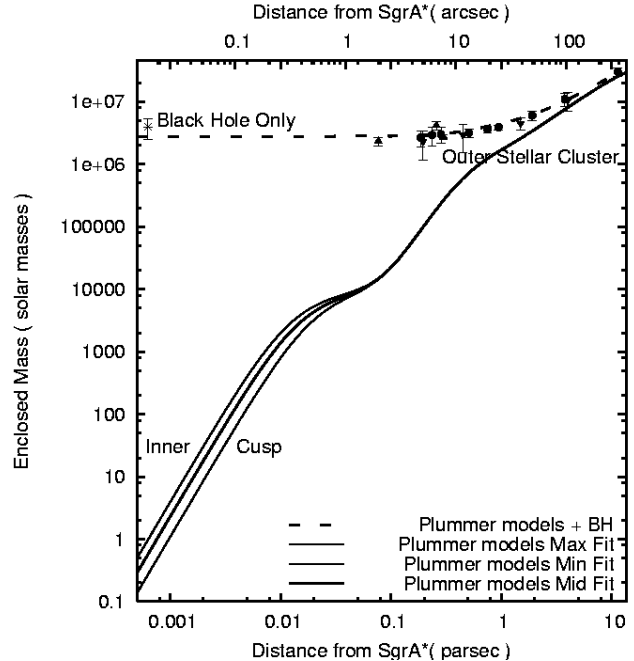


Fig. 2. Mass distribution in the central 10 pc of the Galactic Centre for an 8 kpc distance (Reid et al. 2003; Eisenhauer et al., 2003). The star point denotes the mass derived from the orbit of S2. The error bar combines the orbital fit and astrometry errors (Eisenhauer et al. 2003). Filled circles are mass estimates from a parameterised Jeans-equation model of the radial velocities of late type stars, assuming isotropy (Genzel et al. 2000, Schödel et al. 2002). We omitted all mass estimators at radii of less than $1''$ since they are affected by the surface mass density of the cusp which had not been taken into account in previous investigations. Filled upward-pointing triangles denote Leonard-Merritt projected mass estimators from a new NTT proper motion data set (Schödel et al. 2002). Filled downward-pointing triangles denote mass estimates from the ionized and neutral gas dynamics (Serabyn & Lacy 1985; Güsten et al. 1987; Lacy et al. 1991; Herbst et al. 1993; Roberts & Goss 1993). A comparison of representative mass models to the measured velocity dispersions is given in Genzel et al. (1996, 2000). The long-dashed line is a fit to the measured enclosed mass against distance. That results from a combination of the mass distributions (see § 2.2) deduced from the composite model fit to the stellar cluster, plus a $2.9 \times 10^6 M_\odot$ black hole. The same model without a point mass is represented by the 3 other curves, they correspond to acceptable models of the stellar cluster within the error bars.

this purpose, we chose a fourth order Hermite integrator derived from the one used in high-accuracy N -body simulations (Aarseth 1999, Spurzem 1999, for an introduction of the Hermite scheme see Makino & Aarseth 1992). The advantage of the Hermite scheme is that it allows a fourth order accurate integration based on only two time steps. Therefore it requires the analytic computation of the time derivative of the gravitational force. This is the point where the integrability of the Plummer model is convenient. We computed the trajectory of S2 around the BH and through the extended mass

Table 2. Characteristic $\tilde{\chi}^2_{tot}$ of our fits. The first column lists the obtained characteristic $\tilde{\chi}^2_{tot}$ for which the resulting orbits are considered to be fitting orbits. The 2nd column expresses the total non-reduced χ^2_{tot} for 33 degrees of freedom ($\tilde{\chi}^2_{tot} = \chi^2_{tot}/33$). When column 3 lists the deviation of the obtained $\tilde{\chi}^2_{tot}$ from the lowest obtained $\tilde{\chi}^2_{tot}$, column 4 corresponds their resulting σ error bars.

$\tilde{\chi}^2_{tot}$	χ^2_{tot}	$\Delta\tilde{\chi}^2_{tot}$	σ
0.68	22.5	0	$< 1\sigma$
0.71	23.5	1	1σ
0.80	26.5	4	2σ
0.95	31.5	9	3σ
1.17	38.5	16	4σ
1.44	47.5	25	5σ

as given by our mass model (see § 2). The presence of an extended mass induces retrograde pericentre-shifts which result in open rosetta shaped orbits.

In total there are ten fit parameters - six orbital elements, the total central mass M_{tot} , the fraction f of the extended mass to the total mass M_{tot} , and the 2-D position P of the central mass. All these values are known within a certain margin. We used the position measurements for S2, the dynamical position of Sgr A* and the 5 line-of-sight velocity measurements as determined by Schödel et al. (2003), Eisenhauer et al. (2003) and Ghez et al. (2003a).

A valid computed orbit has to fit both the measured velocities and positions. Therefore, two reduced $\tilde{\chi}^2$ values, one for the positions, $\tilde{\chi}^2_{pos}$, and another for the velocities, $\tilde{\chi}^2_{vel}$, were estimated. While fitting the orbits, we considered the $\tilde{\chi}^2_{pos}$ values for the positions and velocities independently because the $\tilde{\chi}^2$ values for the velocities were, in general, relatively much smaller than for the positions. In some cases they indicated that measurement errors were systematically overestimated. This way, it was possible to attain, both in velocities and in positions, a similar fit quality. Under this condition, it is always possible to define a common $\tilde{\chi}^2_{tot}$ by adding both the $\tilde{\chi}^2$ values obtained from the positions and the velocities. The total reduced $\tilde{\chi}^2_{tot}$, $\tilde{\chi}^2_{tot}$, is simply the χ^2_{tot} divided by the number of degrees of freedom which is equal to 33 in our case. Table 2 lists obtained total reduced $\tilde{\chi}^2_{tot}$ and non-reduced χ^2_{tot} which indicated errors $\leq 5\sigma$. These errors were estimated by applying a deviation $\Delta\tilde{\chi}^2_{tot}$ from the lowest obtained $\tilde{\chi}^2_{tot}$. In our following analysis we used orbital fits with an error $\leq 1\sigma$.

3.1. Influence of model parameters

In order to study the main effects of a varying cusp mass on the orbit of the star S2 we investigated a representative coverage of the parameter space that includes the full range of possible scenarios. In each single orbital run, the total central mass, M_{tot} and its position as well as the extended mass fraction, f , were fixed; only the 6 orbital elements are varied. The three parameters, M_{tot} , the central mass position and f , were varied independently forming a fully representative 3-D grid. In total ~ 360 orbits were computed

and fitted to the data. In the following, we give a short description of this parameter space:

The total mass M_{tot} , together with the the three velocities and three coordinates determine the **orbital elements**. From the imaging data, sky positions and proper motions are given in a certain error range for each epoch. For a chosen initial epoch, these six input values are varied within their observational uncertainties. Our minimization method is a grid scheme, which, although expensive in computing time (time $\propto N^6$, N being the number of steps per parameter), is a robust method which does not fall easily on local minima. Choosing an appropriate N for each parameter, χ^2 values were computed and a 6-D grid was constructed. Ultimately, the lowest χ^2 value determines the best fitting orbit.

The black hole is treated as a point mass with the extended component being centered on it. The lower central mass limit (Reid et al. 2003) and upper central mass limit (Ghez et al. 2003; Schödel et al. 2003) are well determined. Based on these earlier works, the **value of the total central mass** is varied between $2.6 \times 10^6 M_\odot$ and $4.8 \times 10^6 M_\odot$, considering six different values of M_{tot} . In addition, for any of these given **total central masses values**, M_{tot} , the effect of various **extended mass fractions**, f , was investigated (see Fig. 4).

We used the position of Sgr A* as determined by Reid et al. (2003) with an uncertainty of 10 mas. The **location of the central mass** was varied at 14 different positions within this error bar. Fig. 3 shows these positions along with their obtained $\tilde{\chi}^2_{tot}$ values. These were fairly distributed around the *offset* position which is the deviation of the focus of the Keplerian orbit from the central radio position the way determined by Eisenhauer et al. (2003). In order to check the accuracy of the focus of the Keplerian orbit, we compare the two positions for the star S2 at the epoch 2002.30 calculated with the orbital parameters given by Eisenhauer et al. (2003) and by Ghez et al. (2003b). From the corresponding positions and uncertainties, an offset of the projected orbital focus given by Ghez et al. (2003) from the one by Eisenhauer et al. (2003) of 0.0 ± 2.9 mas East and 0.8 ± 2.0 mas North can be derived. Hence, we find an excellent agreement between the two independent results.

In order to take into account the uncertainty of the **core radius of the inner cusp**, the orbital fits computed for our best fitting model value of $R_1 = 15.5$ mpc, were repeated only in the case of the fitting orbits with an error $\leq 2\sigma$, for the extreme cases of $R_1^{min} = 13.2$ mpc and $R_1^{max} = 20.2$ mpc.

4. Results of non-Keplerian fits

4.1. Orbits with lowest $\tilde{\chi}^2_{tot}$ values

Our results show that the available data on the path of S2 can be fitted very well with **non-Keplerian orbits**. However, at present the orbit of S2 is not sufficiently well determined to exclude a pure Keplerian orbit (see Fig. 6). In fact, in both cases a minimum $\tilde{\chi}^2_{tot}$ value of ~ 0.7 was obtained. In other words, it cannot be excluded that there exists an extended mass component in addition to the black hole. In the case of

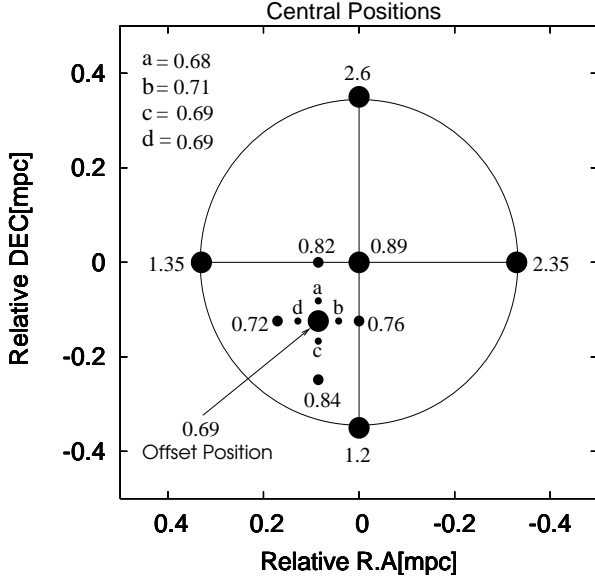


Fig. 3. The different positions of the central mass as they were considered associated with the lowest obtained $\tilde{\chi}^2_{tot}$ value at each given position. The *offset* position is centred in the area showing the lowest $\tilde{\chi}^2_{tot}$ values.

Keplerian orbits and for different central mass position, fits for a $3.65 \times 10^6 M_\odot$ black hole shows the lowest $\tilde{\chi}^2_{tot}$ value. If we assume an additional extended mass component, the lowest $\tilde{\chi}^2_{tot}$ values corresponded to fits for a total mass of $3.65 \times 10^6 M_\odot$ of which 5% are extended or a $4.1 \times 10^6 M_\odot$ total mass of which 10% or 15% are extended, or $4.45 \times 10^6 M_\odot$ total mass of which 20% are extended, as well as a $4.8 \times 10^6 M_\odot$ total mass of which 25% are extended. We can also consider only the fraction of the cusp mass $M_{S2_{apo}}$ which is located at distances from the MBH smaller than the apocenter of the S2 orbit. In this case the 25% limit corresponds to

$$M_{S2_{apo}} / (M_{BH} + M_{S2_{apo}}) \leq 0.05.$$

The orbital parameters for these $\leq 1\sigma$ fitting orbits are given in Appendix A together with the full parameter range that produces orbits with an error of $\leq 5\sigma$. Within the uncertainties the orbital parameters for the Keplerian case agree with earlier work (Schödel et al. (2003), Ghez et al. (2003), Eisenhauer et al. (2003)).

4.1.1. Position of Sgr A*

Only orbits with focuses at *a*, *b*, *c*, *d* and *offset* positions (see Fig. 3 and Fig. 5) resulted with an error of $\leq 1\sigma$. This gives a constraint on the SMBH black hole position of only a separation of ± 0.05 mpc (± 1.3 mas) in R.A or in Dec. from the *offset* positions.

4.1.2. Higher total central masses and cusp masses

Fig. 4 shows a plot of $\tilde{\chi}^2_{tot}$ vs. different discrete central total mass values and for each fraction *f* of the extended mass at the offset position. We also examined orbits with total masses higher than $4.8 \times 10^6 M_\odot$, up to $11.6 \times 10^6 M_\odot$. We found that

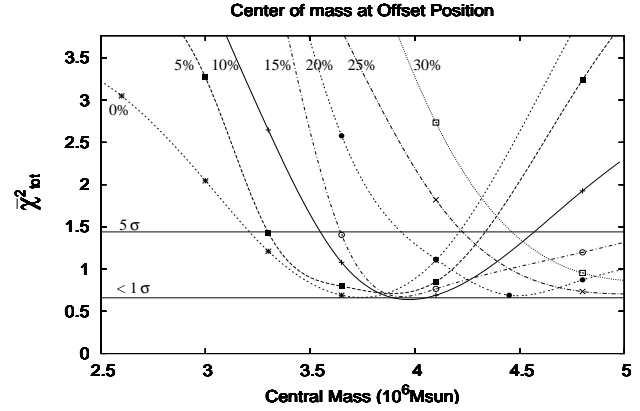


Fig. 4. Plot of the $\tilde{\chi}^2_{tot}$ values vs. the total central mass, M_{tot} , calculated for different extended mass fractions, *f*, with the point mass at the *offset* position. Values of the same *f* are fitted with splines. Crosses: *f* = 0; “x” symbols: *f* = 0.05; stars: *f* = 0.1; empty squares: *f* = 0.15; filled squares: 0.2; empty circles: *f* = 0.25; and filled circles: *f* = 0.3. The two horizontal lines denoted by $< 1\sigma$ and 5σ delimit the region of fitting orbits ($\tilde{\chi}^2_{tot} \leq 1.44$).

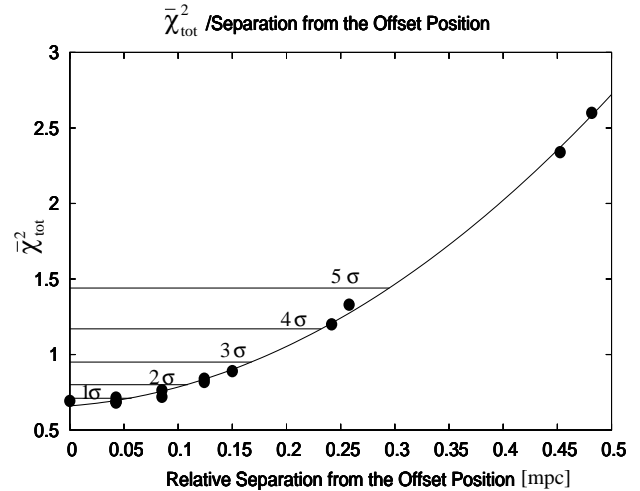


Fig. 5. The lowest obtained reduced $\tilde{\chi}^2_{tot}$ values in function of the separation from the *offset* position. These are fitted with a function of the form $7.2x^2 + 0.5x + 0.7$.

at a 5σ level of confidence the S2 orbit could fit the data for cusp masses of up to 70% of the total mass. This resulted in an upper limit of cusp masses as high as $8 \times 10^6 M_\odot$ corresponding to an extended component of $\sim 1 \times 10^6 M_\odot$ inside the sphere of a radius equal to the apocentre of S2. However, the total masses in these cases are in disagreement with the dynamical mass estimates at large radii. Therefore, we regard them as unrealistic but mention the result for completeness.

Large amounts of extended mass inside the S2 orbit would be possible if the mass distribution function at the centre were steeper than in our model or if the core radius were smaller than the apo-centre of S2 (~ 9 mpc). In that case we found that mass densities – exceeding the currently derived few $10^8 M_\odot \text{pc}^{-3}$ by three or four orders of magnitude – are

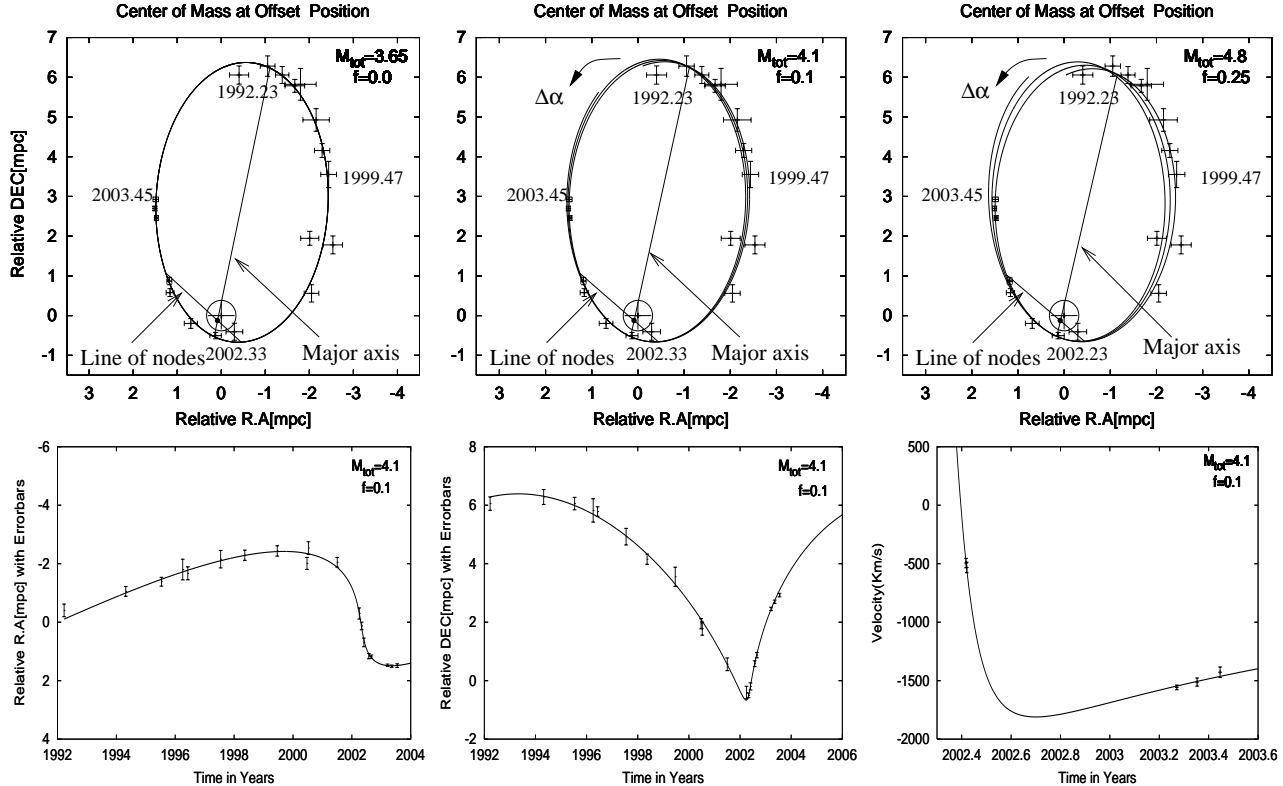


Fig. 6. Three exemplary orbits determined by our fitting. Upper left panel: Keplerian orbit with $3.65 \times 10^6 M_\odot$ point mass. Upper middle panel, non-Keplerian orbits with $4.1 \times 10^6 M_\odot$ total mass, thereof 10% extended. Upper right panel, non-Keplerian orbits with $4.8 \times 10^6 M_\odot$ total mass, thereof 25% extended. Here the central mass is at the offset position, 0.09 mpc east and 0.12 mpc south from the nominal radio position of Sgr A*. The lower panels show the velocity in the relative R.A., the relative Dec., and along the line-of-sight as a function of time for the case of $4.1 \times 10^6 M_\odot$ total central mass with a 10% extended component. This case is representative for the other cases. The direction of $\Delta \alpha$ the pericentre-shift is shown by an arrow.

unlikely to form a stable configuration because stellar collisions will become of increasing importance (see section 5.2).

4.1.3. Core radius and slope of the density profile

In the case of the *offset* position, for all the orbits with errors $\leq 2 \sigma$, the fitting procedure was repeated for the extreme cases of $R_1^{\min} = 13.2$ mpc and $R_1^{\max} = 20.2$ mpc of the inner cusp radius. Even with these different core radii, the case of the *offset* position is found to give the lowest $\tilde{\chi}^2_{\text{tot}}$ values. Also the fit quality remains unchanged at $\tilde{\chi}^2_{\text{tot}} \approx 0.7$. We also consider that the compact component can have a much smaller core radius than the stellar profile, possibly well within the S2 apocentre. In this case, following the result of Rubilar & Eckart (2001, see their Fig.5), we deduce that for the same extended mass fraction, f , the induced pericentre-shift is smaller for a bigger core radius. Thus for a core radius that does not exceed a value 15.5 mpc, our estimation on the mass of the cusp is an upper limit.

Using a series of Plummer model density profiles, implies a value of the cusp slope of $\alpha \leq 5$. As mentioned in § 2, Genzel et al. (2003) fitted the stellar number density with a broken power-law of a slope equal 1.4 ± 1 . From theoretical models of cusps around massive black holes, one would

expect power-law indices in the range $3/2 \leq 7/4$ (Bahcall & Wolf 1977; Murphy et al. 1991). To study the influence of the density profile on the pericentre-shift, we performed fittings of the S2 orbit considering a power-law profile of a slope equal to 1.4. The pericentre-shift induced by the same amount of mass inside S2's apocentre but different fractions of mass, f , did not exceed the one induced by a Plummer model density profile by more than 12%. Thus, by covering a wide range of slopes $1.4 \leq \alpha \leq 5$, we found that for the shallower mass distribution, the pericentre-shift never exceeds 12% of our initially derived value, thus our estimates indicate an upper limit on the mass that could be present inside the S2 apocentre, and consequently on the mass of the cusp.

5. Discussion

In the previous sections it was demonstrated that the measured positions and line-of-sight velocities of S2 are not sufficiently well determined to exclude a Keplerian orbit. Assuming a simple Keplerian case, the central gravitational potential by definition is entirely dominated by the point mass associated with Sgr A* and no dynamical constraints can be derived on any extended mass component due to e.g. the surrounding

stellar cluster. More revealing, however, is the more physical assumption of non-Keplerian orbits. The presence of a stellar cusp shows that – at least to a certain extent – there is some extended mass present near the black hole. This potential can be modelled by a central black hole plus an extended mass component. We assumed that the cusp has the same shape as the observed stellar number density counts which we fitted by a Plummer density model (see §2). We also took into account that the total enclosed mass at larger radii (1pc) would not exceed a value of $\sim 4.8 \times 10^6 M_{\odot}$ (see section 3.1).

Having shown that the current data allow for an extended mass component higher than the one of $8540 M_{\odot}$ inferred from stellar number density counts which were scaled to match the velocity distribution at large radii (see §2), we will discuss its nature in sections §5.1 and §5.2. The value of $8540 M_{\odot}$, representing the total mass of the ‘inner cusp’, is equivalent to a mass of $3100 M_{\odot}$ inside the core radius R_1 (15.5 mpc or $0.4''$). It is based on the assumption that the ratio of the stellar number counts to total stellar mass does not vary with radius and environment in the Galactic Centre, i.e. that the mass-to-light ratio $M/L(2\mu\text{m})$ is constant (see also Genzel et al., 2003). It is very likely that this assumption is unjustified. Genzel et al. (2003) find that the stellar population in the cusp differs to a certain degree from the population of the surrounding, large-scale cluster. Also, effects such as mass segregation and stellar collisions might work very effectively in the dense environment of the cusp and M/L would show higher values towards the centre (Baumgardt et al. 2003). Therefore, we consider that the mass-to-light ratio, $M/L(2\mu\text{m})$ of the ‘inner cusp’, can be different from that of the outer stellar cluster. In the following, two hypotheses will be discussed: The existence of a cluster of faint low-mass stars, not yet detectable with the resolution and sensitivity of current instruments, and the existence of a cluster of heavy dark objects like stellar black holes and neutron stars.

5.1. Extending the K-band Luminosity Function to Faint Stars

We use the K-band luminosity function (KLF) for $K \leq 18$ mag within a projected radius of $1.5''$ from Sgr A* as it was determined by Genzel et al. (2003 - see their Fig.11). Note that the KLF is not corrected for extinction or for the distance modulus. The authors fitted the KLF with a power-law with a slope of $\beta = 0.21 \pm 0.03$, ($\beta = d \log N / dK$). Since this result is based on a number of roughly 60 stars within $1.5''$ of Sgr A*, the observed stars themselves cannot account for a significant extended mass component. It is therefore necessary to extrapolate the KLF at the faint end. However, we assume that the observed stars trace the mass carrying population which can currently only be accessed theoretically by extrapolating the KLF towards its faint end.

For the extrapolation of the KLF two different slopes are considered, $\beta = 0.21$ and a steeper one, $\beta = 0.35$, which fits the Bulge KLF (Alexander & Sternberg, 1999) as well as a model of an old (~ 10 Gyr) stellar cluster of solar metallicity (Zoccali et al. 2003). In the following we concentrate on the region within R_1 of the inner Plummer model component. The total number of stars in the inner cusp ($R \leq 0.4''$

Table 3. Extinction free mass-to-light ratios, $M/L(2\mu\text{m})$, for different stellar types in luminosity class V at the distance of the Galactic Centre.

$M/L(2\mu\text{m})[M_{\odot}/L_{\odot}]$	K[mag]	Mass[M_{\odot}]	Spectral types
1.29	16.425	1.60	F0
1.93	17.005	1.40	F5
2.73	17.695	1.05	G0
5.02	18.665	0.79	K0
5.36	18.915	0.67	K5
11.77	20.065	0.51	M0
9.23	20.065	0.4	M2
16.66	20.915	0.33	M3
38.49	22.315	0.21	M5
87.55	23.815	0.12	M7
166.43	25.265	0.06	M8

or 15.5 mpc) brighter than a given magnitude can be directly estimated from the (extrapolated) KLF.

The KLF gives the number of stars per surface area per magnitude. In order to calculate the total number of stars and the total stellar mass present within the spherical volume enclosed by the core radius of $R = 0.4''$ of our central Plummer model component, we de-projected the KLF. Table 4 lists the resulting numbers of stars, the total cluster mass, M_{Cl} , the average stellar mass in the cluster, M_{aver} , and the corresponding $M/L(2\mu\text{m})$ for clusters given by KLFs with slopes of $\beta = 0.21$ and $\beta = 0.35$ and for different cut-off magnitudes, between $K = 20$ ($M_{min} = 1M_{\odot}$) and $K = 28$ ($M_{min} = 0.06M_{\odot}$). M_{Cl} is calculated from the observed KLF using $A_K = 3$ and the $M/L(2\mu\text{m})$ values listed in Table 3.

The numbers listed in Table 4 show that the mass of stars present within $R = 0.4''$ deduced from a $\beta = 0.21$ slope KLF cannot be higher than $800 M_{\odot}$, even after extrapolation to the faintest magnitudes (see Table 3 for a list of K-magnitudes and 0.1051 corresponding MS-stars at the GC). Therefore, a cluster with a KLF of $\beta = 0.21$ cannot explain a mass of $3100 M_{\odot}$ within $R = 0.4''$, estimated from direct number density counts with an $M/L(2\mu\text{m}) = 2 M_{\odot}/L_{\odot}$ (see § 2).

$M/L(2\mu\text{m})$ converges to a value $2 M_{\odot}/L_{\odot}$ for $\beta = 0.35$, and a magnitude limit between 26 and 27, in this case we find the value of $3100 M_{\odot}$ required by our mass distribution modelling in §2. Lower magnitude limits would increase $M/L(2\mu\text{m})$ further, and the mass of the inner cusp calculated from our Plummer model would be underestimated. Stellar types corresponding to the required $M/L(2\mu\text{m})$ ratios are listed in Table 3.

Table 4 also shows that for a main-sequence stellar population $M/L(2\mu\text{m})$ does not exceed $4.0 M_{\odot}/L_{\odot}$, even if we consider very faint/low-mass stars ($K = 28$) and a steep faint-end KLF ($\beta = 0.35$). This value corresponds to a cusp representing only 0.2% of the total mass (see Table 5). We conclude that the amount of extended mass allowed inside the core radius of the ‘inner cusp’ would be far too large to be explained by a stellar population of MS stars, and therefore would require another type of mass carriers. We show in § 5.3 that such a configuration is possible.

Table 4. For each ‘observed’ K-magnitude limit (not corrected for extinction) we give the numbers of stars N , cluster mass M_{Cl} , average stellar masses M_{aver} , and mass-to-luminosity ratio, $M/L(2\mu\text{m})$, within the central $0.4''$ for hypothetical Plummer model type clusters with KLFs extrapolated by two power-law slopes of $\beta = 0.21$ and $\beta = 0.35$. M_{Cl} is the mass inside the core radius R_1 of the innermost Plummer model component. The derived M/L values include an extinction correction for $A_K=3$.

Magnitude limit	$\beta=0.21$				$\beta=0.35$			
	N	$M_{Cl}[M_\odot]$	$M_{aver}[M_\odot]$	$M/L(2\mu\text{m})[M_\odot/L_\odot]$	N	$M_{Cl}[M_\odot]$	$M_{aver}[M_\odot]$	$M/L(2\mu\text{m})[M_\odot/L_\odot]$
$K \leq 28$	3500	800	0.9	1.0	44500	5200	0.1	3.7
$K \leq 27$	2200	710	1.4	0.9	20000	3700	0.15	2.8
$K \leq 26$	1350	620	2.3	0.8	9000	2400	0.3	1.8
$K \leq 25$	820	525	3.7	0.7	4100	1500	0.8	1.1
$K \leq 24$	510	450	6.0	0.6	1920	1000	1.6	0.8
$K \leq 23$	310	390	10	0.5	950	700	3.3	0.5
$K \leq 22$	190	325	16	0.4	510	480	6.0	0.4
$K \leq 21$	120	235	26	0.4	320	380	9.7	0.3
$K \leq 20$	70	193	42	0.3	230	270	11.2	0.2

Table 5. Mass-to-light ratios $M/L(2\mu\text{m})$, for the different *off-set* position fitting orbits obtained from our model calculations. The errors on M/L are model dependent. From scaling to the enclosed mass estimate in Fig. 2 we estimate an error of 5%. Columns 3, 4, and 5 give the cusp mass inside the orbit of S2 for core radii of respectively 20.2mpc, 15.5mpc and 13.2mpc.

M_{rot} [$10^6 M_\odot$]	f	M_{S2apo} $R_1 =$ 20.2mpc	M_{S2apo} $R_1 =$ 15.5mpc	M_{S2apo} $R_1 =$ 13.2mpc	$M/L(2\mu\text{m})$ [M_\odot/L_\odot]
3.65	0.0	0.001	0.001	0.001	2.00
3.65	0.05	0.011	0.021	0.031	42.74
3.65	0.10	0.022	0.044	0.062	85.48
4.10	0.05	0.013	0.024	0.033	48.01
4.10	0.10	0.025	0.049	0.071	96.02
4.10	0.15	0.038	0.071	0.104	144.03
4.10	0.20	0.052	0.098	0.140	192.04
4.45	0.20	0.049	0.105	0.155	227.7
4.80	0.20	0.061	0.108	0.157	224.82
4.80	0.25	0.069	0.135	0.190	269.32
4.80	0.30	0.089	0.164	0.237	337.24

5.2. Stability of a Cluster of Low-Mass Stars

For a multi-mass stellar distribution, high mass stellar remnants (stellar black holes and/or neutron stars) are expected to migrate to the centre as a consequence of dynamical friction. One would expect that, within a Hubble time, these compact objects show a higher concentration toward the centre than the lighter ones (Morris et al., 1993; Miralda-Escudé & Gould, 2000), which should be transferred by that mechanisms to orbits at greater distances from the centre of the cluster. This argues against the existence of a cluster of low-mass stars in the inner cusp.

On the other hand, the possibility of a cluster of low-mass stars cannot be excluded and we are far from understanding the properties of the stars in the cusp. There is for example the unexplained presence of massive young stars, e.g. MS O/B-type stars close to the black hole (Genzel et al., 1997; Eckart, Ott & Genzel, 1999; Figer et al., 2000; Gezari et al., 2002; Ghez et al., 2003). These stars have not had enough time to

achieve energy equipartition with the fainter older stellar population. They are hence dynamically un-relaxed. Also, there are indications for a radial anisotropy of the stars in the cusp which might be un-relaxed (Schödel et al., 2003), in spite of the expected short relaxation time in this dense environment. Because of this general lack of theoretical understanding of the cluster near Sgr A*, we consider that a cluster of faint/low mass stars should not be ruled out entirely from the possible interpretations of the inner cusp.

5.3. Is the Cusp Dominated by Dark and Massive Objects?

In this section, we consider orbital fits with errors of $\leq 1\sigma$ that result in high cusp masses yet are in good agreement with the enclosed mass measurements. The evaluation presented in § 5.1 shows that such a heavy cusp is unlikely to consist of stars only. Here we study whether such a cusp could consist of heavier mass carriers like stellar black holes or neutron stars.

5.3.1. Presence of stellar remnants in the center due to dynamical friction

When the compact remnants of massive stars are themselves significantly more massive than the normal field stars in the Galactic Centre, as would be the case of black hole remnants, than they are susceptible to inward migration as a consequence of dynamical friction. The resulting mass segregation can lead to a pronounced concentration of compact objects within the central stellar core within a Hubble time (Morris, 1993). N -Body simulations of globular clusters showed that the combination of stellar evolution (production of stellar mass black holes, neutron stars, white dwarfs, and of binaries including such objects) and stellar dynamics will almost certainly lead to a strong increase of M/L in the central parts of the nuclear star cluster. Black holes and neutron stars sink to the centre and may coalesce (Gürkan et al. 2003). Such highly detailed self-consistent simulations of the dynamical episodes are, however, not yet possible on the scale of the Galaxy. N -Body simulations (even with cutting-edge special

purposes computers like GRAPE-6 (Makino 2001)) cannot follow the evolution of a galactic nucleus over a Hubble time if relaxation is appreciable (Freitag & Benz, 2002).

Under certain assumptions and for some range of initial parameters, less realistic but more efficient Monte Carlo numerical simulations of the evolution of the GC (Freitag & Benz, 2002) showed that the SBHs sink to the center on a short timescale of a few gigayears, settle into a centrally concentrated distribution and dominate the stellar mass there. Similarly, Murphy Cohn & Durisen (1991, see their figure 8b) showed that densities higher than $10^9 M_\odot \text{pc}^{-3}$ could reside in regions as close as few mpc from the central SBH. Other studies by Morris (1993) and Miralda-Escudé & Gould (2000) estimate that $10^4 - 10^5$ SBHs, due to dynamical friction, would have accumulated at distances of less than about 1 pc from the center. These latter works can only account for about $10^2 - 10^4 M_\odot$ within separations of about 20 mpc from the centre which represents only 1% to 10% of our upper mass limit derived from the orbit of S2. However, the central density of the SBH cluster depends on various uncertain quantities: the SBH mass function, the stellar IMF and formation rate, the remnant progenitor masses, and the dynamical age of the GC. Morris (1993) argued that within a wide range of assumptions about the IMF, and about the minimum stellar mass capable of producing a black hole remnant, the total mass of remnants concentrated into the inner few tenth of a parsec, would be about $0.4-5 \cdot 10^6 M_\odot$. If the black hole remnants were to achieve equipartition with the field stars, they would form an inner core with a radius of a size as small as 50 mpc. These would coalesce or form a quasi-stable cluster of stellar mass black holes. Even if a catastrophic merger of stellar remnants did occur at some point at the age of the galactic nucleus, the continuous influx of massive stellar remnants would ensure that a concentrated population of them is present within the stellar core. These findings apply, however, in the absence of an initial central black hole. To our knowledge, a similar study of a cluster with already a pre-existing super-massive black hole, as in the centre of our Galaxy, is not yet available.

5.3.2. In situ formation of stellar remnants

In the case of the Galactic Centre, complex dynamical episodes have taken place. A numerous variety of young early-type, bright and massive stars exist at distances of 10 mpc - 400 mpc from the centre. There exist a dozen of bright O/B main sequence stars within about 40 mpc of Sgr A*, these are fast moving S-stars (mass $\sim 20 M_\odot$) of which the star S2 is an example. There exists also ~ 30 more massive ($30 M_\odot \lesssim \text{mass} \lesssim 100 M_\odot$) very bright early-type stars, the so-called He stars exhibiting He/HI emission lines. The existence of these two types of stars at these regions from the center is still not understood. These could have formed there or would have migrated there due to different in-spiraling processes (Genzel et al. 2003; Ghez et al. 2003; Gerhard et al. 2001, Krabbe et al. 1995). If such stars were always present in the center of the Galaxy, due to stellar evolution, their remnants would contribute very efficiently to the

formation of a dense cluster also at the center. Here, we assume that these stars would end their lives in the formation of neutron stars or stellar black holes with masses between $1.5 M_\odot$ and $10 M_\odot$ (on average $7 M_\odot$), we also consider their lifetimes to be $\lesssim 10^7$ yrs. If after a single lifetime about 40 of such stars form stellar remnants, throughout the age of the Galaxy ($\sim 10^{10}$ yrs), it is possible to account for about $10^5 M_\odot$ needed to explain our upper mass limit of the 'inner cusp'.

Considering the two above described scenarios - while these do not represent the complete history of the galactic nucleus - it is, however, a fair conclusion that *strong to moderate* dynamically caused M/L variations prevail at the GC.

Our attempts in this work is not to explain the formation of a high density cluster of stellar remnants at the GC. We would rather like to analyse such a configuration if existent. In the following we investigate if such a hypothetically high M/L configuration of stellar remnants can form a stable configuration.

5.3.3. Stability of a cluster of stellar remnants

Rauch & Tremaine (1996) studied the configuration of a central massive black hole plus an extended mass distribution M of radius R consisting of objects with mass m in terms of its *non-resonant* relaxation time t_{rel}^{nr} . Under the assumption that $M \ll M_{BH}$, Rauch & Tremaine (1996) derive how t_{rel}^{nr} depends on M_{BH} , M , and the orbital time scale t_{orb} at the outer edge of the cluster. If (a) the stellar orbits have random orientations and moderate eccentricities, (b) the density of stars is approximately uniform within R , and (c) $M_{cluster} / M_{BH} = 10^{-2} - 10^{-5}$ then Rauch & Tremaine (1996) find that

$$t_{rel}^{nr} \sim \frac{M_{BH}^2}{m^2 N \ln \Lambda} t_{orb}, \quad (5)$$

where $\ln \Lambda$ is the Coulomb logarithm ~ 13 in this case. This situation should - to first order - be applicable to the Black Hole/cusp scenario at the Galactic centre. Condition (a) is probably fulfilled with the possible exception that the stars in the cusp might have fairly high eccentricities (Schödel et al. 2003). Assuming a Plummer model as a cusp description fulfills condition (b). We consider the case where a pericentre-shift of the order of 1° is induced. As an example, we choose the case of a cusp mass of 15% with a total mass of $4.1 \times 10^6 M_\odot$. This cusp mass is well below the upper limit derived in section 4.1. In the case of a cusp mass of 15%, M/M_{BH} is of the order of 10^{-2} , if we restrict ourselves to the region within the core radius R_1 . This is close to what is required by condition (c).

Here, $M_{BH} = 3.5 \times 10^6$ and m_{sr} is the average mass of the stellar remnants. A value of $m_{sr} = 5 M_\odot$ is roughly consistent with a composite cluster made of neutron stars ($m \sim 1.5 M_\odot$) and stellar black holes ($5 M_\odot < m < 25 M_\odot$). We then find that $t_{rel}^{nr} \sim 10^6 \times t_{orb}$, if we assume that most of the mass inside the core radius is present in the form of stellar remnants of average mass m_{sr} . Considering that the core radius of 15-20 mpc will define t_{orb} we find t_{rel}^{nr} to be about 2×10^7 years.

We can also investigate whether such a configuration is stable by estimating how many stellar black holes evaporate. Integrating a Maxwell distribution function for the velocities above the escape velocities gives the percentage of stars not bound to the BH. For the velocity dispersion, following Alexander et al. (2003), we can write:

$$v_{\text{escape}} = \sqrt{2}v_{\text{circular}} = \sqrt{2(1+\alpha)}\sigma. \quad (6)$$

For a value of $\alpha = 2$, about 0.03% of the present stellar black holes will be evaporated after each relaxation time. For a steeper cusp with $\alpha=3$ we find that 0.006% of the stellar black holes will evaporate on that time scale. For $t_{\text{rel}}^{\text{nr}}$ of a few 10^7 years and α between 2 and 3 about 50% of the stellar black holes will have evaporated after 25 to 250 $t_{\text{rel}}^{\text{nr}}$ corresponding to about 5×10^8 to 5×10^9 years. Given the fact that there will also be an influx of mass i.e. stellar black holes or neutron stars from outside the cusp one can consider such a configuration stable over a significant fraction of the Milky Way's age.

Given equation (5), for a fixed t_{orb} , the relaxation time decreases linearly with N , i.e with the cusp mass. Thus, cusp masses well exceeding $2 \times 10^5 M_{\odot}$ would not form a stable configuration compared to the age of the Milky Way.

6. Summary

From stellar number counts, we have a strong reason to assume that there is some extended mass around Sgr A*. Therefore, orbits of stars near Sgr A* should be analyzed in terms of non-Keplerian motion. Only in that way it is possible to find out more about the composition of the cusp. This paper presents the first approach to this problem. In this work we studied the case where the contribution of the central stellar cluster at the centre of the Milky Way could introduce peri-centre-shifts of the order of 1 degree per revolution on the orbit of S2. We assume that the dynamics of S2 is governed by both the super-massive black hole and the central cluster. The steeply rising, cusp-like stellar density distribution in the inner few tens of milli-parsecs near Sgr A* can be modeled with a Plummer model distribution having a relatively small core radius of the order of the S2 semi-major axis. In a spherical potential, the stellar orbits will precess and the stars will follow rosetta shaped trajectories (Binney & Tremaine, 1987; Rubilar & Eckart, 2001; Fragile, & Mathews, 2000). We performed orbital fits to the S2 data for this class of orbits. We used a fourth order Hermite integrator, adequate for the required precision. The runs were performed for a large range of initial parameters for the total mass, the position of the centre of mass, the fraction of the extended mass component, and the 6 classical orbital parameters.

We found that the S2 trajectory can be equally well fitted by *non-Keplerian* orbits as by *Keplerian* orbits. For the Keplerian case, we could confirm the results of Schödel et al. (2003), Ghez et al. (2003), and Eisenhauer et al. (2003). Basically independent of the amount of total or extended mass we find consistently a value for the central Black Hole mass of about $3.7 \times 10^6 M_{\odot}$. This is well between but not coincident with one of the two possible Black Hole mass estimates

of either $4.75 \times 10^6 M_{\odot}$ or $2.79 \times 10^6 M_{\odot}$ that were derived by Aschenbach et al. (2003) from an analysis of the quasi-periodicity observed in strong X-ray flares.

A *non-Keplerian* orbit with a fit error of $\leq 1\sigma$ that shows a peri-centre-shift of the order of 1° implies a total mass of $4.1 \times 10^6 M_{\odot}$ with a fraction of the extended mass being $f = 0.15$. With this value of f , the amount of mass present in the inner cusp is ~ 75 times larger than the one expected from a direct mass estimation deduced from the stellar density and the integrated mass plot (see Fig. 1 and Fig. 2) while assuming a constant $2\mu\text{m}$ mass-to-light ratio of $2 M_{\odot}/L_{\odot}$.

If the inner cusp is mainly composed of main sequence stars, then a $M/L(2\mu\text{m})$ of $2 M_{\odot}/L_{\odot}$ can only be attained in the case of a faint-end KLF slope of $\beta = 0.35$ and a magnitude limit $25 < K < 26$. The mass of such a cluster will be $3100 M_{\odot}$ within $R = 15$ mpc derived from our initial Plummer model in § 2. The existence of even fainter ($K < 28$), low-mass stars ($0.06 M_{\odot}$) in the inner cusp will not contribute more than ~ 3 times the mass in the inner cusp; such a configuration is not likely to be stable for a long time. In addition it would be unclear how these stars would get into the inner cusp. It is unlikely that they formed there, however, they might have migrated into that region by losing angular momentum by interactions with stars in the overall Galactic Centre stellar cluster with a core radius of 0.3-0.4pc.

The example of a total mass of $4.1 \times 10^6 M_{\odot}$ and an extended mass component of 15%, as discussed above, implies an $M/L(2\mu\text{m})$ of $\sim 145 \pm 10 M_{\odot}/L_{\odot}$; here objects with large M/L values are needed to explain the extended cusp mass. One plausible explanation could be the presence of a cluster of massive stellar remnants. By applying equation. 5, we find that an equilibrium configuration is possible under certain conditions.

In this study relativistic effects were not included for the orbit of the star S2. The peri-centre-shift induced by relativistic effects is of the order of 9 arcmin compared to the 40 arcmin expected from the Newtonian shift due to the presence of an extended mass (see also Rubilar & Eckart, 2001, Fragile, & Mathews, 2000). It should be pointed out that the peri-centre-shift due to relativistic effects is in the opposite direction of that due to the extended mass and that relativistic effects could in a way mask the amount of extended mass around the black hole. Therefore it will be important for future work to investigate relativistic effects in more detail.

After only a few additional observational epochs it will be possible to put even stronger constraints on the mass of the cusp, and consequently to know more about the mass carrying population in the immediate vicinity of the black hole at the centre of the Milky Way.

As discussed in Rubilar & Eckart (2001) a complete determination of the cusp parameters can be expected from combinations of 3 or more orbits since then the number of degrees of freedom for the fits is increasing rapidly. Further studies with more general density distributions should be undertaken, because they may influence the precise value of the extended mass contribution.

Appendix A: Orbital parameters of three 1σ fitting orbits

In table A.1, we give the orbital parameters of 3 exemplary orbits giving fits within a 1σ limit. The orbits corresponding to those fits are plotted in Fig.6. These are chosen for the case where the central black hole is present at the *offset* position ((R.A = 0.09 mpc; Dec = -0.12 mpc) from the central nominal radio position of Sgr A*). We also give the full range of parameters [Min;Max] which gives fits corresponding to a 5σ level. Here, we exclude solutions with $M_{tot} > 5.4 \times 10^6 M_{\odot}$.

Acknowledgements. N. Mouawad thanks M. Freitag for substantial discussions. This work has been partly supported by the Deutsche Forschungsgemeinschaft (DFG) via grant SFB439 at the University of Heidelberg and SFB494 at the University of Cologne.

References

- Aarseth, S.J. 1999, Pub. Astron. Soc. Pac , 111, 1333
 Alexander, T. 1999, ApJ, 527, Issue 2, 835
 Alexander, T. & Sternberg, A., 1999, ApJ, 520, 137A
 Alexander, T. 2003, In: The Galactic black hole. Lectures on general relativity and astrophysics. Edited by Heino Falcke; Friedrich W. Hehl. Series in high energy physics, cosmology and gravitation. Bristol: IoP, Institute of Physics Publishing, ISBN 0-7503-0837-0, 2003, p. 246-274
 Aschenbach, B., Grosso, N., Porquet, D., Predehl, P., A&A accepted, astro-ph/0401589
 Bahcall, J., N. & Wolf, R. A. 1977, ApJ, 216, 883b
 Baumgardt, H., Hut, P., Makino, J., McMillan, S., & Portegies Zwart, S. 2003, ApJ , 582, L21
 Binney, J. & Tremaine, S. 1987, Galactic Dynamics, Princeton Series in Astrophysics
 Eckart, A., Genzel, R., Hofmann, R., Sams, B. J. & Tacconi-Garman 1995, ApJ, 445, L23
 Eckart, A. & Genzel, R. 1996, Nature, 383, 415
 Eckart, A., Ott, T., Genzel, R. 1999, A&A, 352L, 22E
 Eckart, A., Genzel, R., Ott, T. & Schödel, R. 2002a, MNRAS, 331, 917
 Eckart, A., Mouawad, N., Krips, M., Straubmeier, C., and Bertram, T., 2002, SPIE 4835-03, Cnf. Proc. of the SPIE Meeting on 'Astronomical Telescopes and Instrumentation', held in Waikoloa, Hawaii, 22-28 August 2002b
 Eckart, A., Bertram, T., Mouawad, N., Viehman, T., Straubmeier, C., Zuther, J. 2002, Contribution to the JENAM meeting on: The VLTI - Challenges for the Future, Porto, Portugal, September 4-7, 2002c
 Eisenhauer, F., Schödel, R., Genzel, R., Ott, T., Tecza, M., Abuter, R., Eckart, A. & Alexander, T. 2003, ApJ, 597, Issue 2, L121
 Ferrarese, L., Pogge, R. W., Peterson, B. M., Merritt, D., Wandel, A., & Joseph, C. L. 2001, ApJ , 555, L79
 Figier, Donald F., Becklin, E. E., McLean, Ian S., Gilbert, Andrea M., Graham, James R., Larkin, James E., Levenson, N. A., Teplitz, Harry I., Wilcox, Mavourneen K. & Morris, Mark, 2000, ApJ, 533L, 49F
 Fragile, P.C. & Mathews, J., 2000, ApJ 542, 328
 Freitag, M. & Benz, W., 2002, A&A, 394, 345
 Genzel, R., Hollenbach, D. J., Townes, C. H., Eckart, A., Krabbe, A., Lutz, D. & Najarro, F.t., 1994, NATO Advanced Science Institutes (ASI), Series C, 445, 327
 Genzel R., Thatte N., Krabbe A., Kroker H. & Tacconi-Garman L. E., 1996, ApJ, 317, 153
 Genzel, R., Eckart, A., Ott, T., & Eisenhauer, F., 1997, MNRAS, 291, 219G
 Genzel, R., Pichon, C., Eckart, A., Gerhard, O. & Ott, T., 2000, MNRAS, 317, 348
 Genzel, R., Schödel, R., Ott, T., Eisenhauer, F., Hofmann, R., Lehnert, M., Eckart, A., Alexander, T., Sternberg, A., Lenzen, R., Clnet, Y., Lacombe, F., Rouan, D., Renzini, A. & Tacconi-Garman, L. E. 2003, ApJ, 594, Issue 2, 812
 Gerhard, O., 2001, ApJ, 546, Issue 1, pp. L39
 Gezari, S., Ghez, A. M., Becklin, E. E., Larkin, J., McLean, I. S., Morris, M., 2002, ApJ, 576, 790G
 Ghez, A. M., Klein, B. L., Morris, M. & Becklin, E. E. 1998, ApJ, 509, Issue 2, 678
 Ghez, A., Morris, M., Becklin, E.E., Tanner, A. & Kremenek, T. 2000, Nature, 407, 349
 Ghez, A., Duchêne, G., Matthews, K., Hornstein, S. D., Tanner, A., Larkin, J., Morris, M., Becklin, E. E., Salim, S., Kremenek, T., Thompson, D., Soifer, B. T., Neugebauer, G., & McLean, I. 2003a, ApJ, 586, L127
 Ghez, A., Salim, S., Hornstein, S. D., Tanner, A., Morris, M., Becklin, E. E. & Duchêne, G. 2003b, astro-ph/0306130
 Gürkan et al. 2003, astro-ph/0308449
 Güsten R., Genzel R., Wright M. C. H., Jaffe D. T., Stutzki J., Harris A. I. 1987, ApJ, 317, 124
 Herbst T. M., Beckwith S. V. W., Forrest W. J. & Pipher J. L., 1993, AJ, 317, 956
 Kormendy, J. & Richstone, D. 1995, Annu. Rev. Astron. Astrophys., 33, 581
 Kormendy, J. 2001, Rev. Mexicana Astron. Astrofis. Ser. Conf., 10, 69
 Krabbe A. et al., 1995, ApJ, 317, L95
 Lacy, J. H., Achtermann, J. M. & Serabyn, E. 1991, ApJ, 380, L71
 Lo, K. Y., 1985, Proceedings of the ESO-IRAM-Onsala Workshop on (Sub)Millimeter Astronomy, Aspenas, Sweden, June 17-20, 1985, 273 sma..work..273L
 Makino, J. & Aarseth, S.J. 1992, Proc. Astron. Soc. Japan, 44, 141
 Makino, J. 2001, in ASP Conf. Ser. 228: Dynamics of Star Clusters and the Milky Way, ed. S. Deiters, B. Fuchs, R. Just, & R. Spurzem, 87
 Maoz, E. 1998, ApJ, 494, 181
 Melia, F. & Falcke, H. 2001, Annu. Rev. Astron. Astrophys. 2001, 39, 309
 Mezger, P. G., Duschl, W. J. & Zylka, R. 1996, Astron. Astrophys. Rev., 7, 289
 Miralda-Escudé, J. & Gould, A. 2000, ApJ, 545, Issue 2, 847
 Morris, M. 1993, ApJ, 408, 496
 Morris, M. & Serabyn, E. 1996, Annu. Rev. Astron. Astrophys. 1996, 34, 645
 Munyaneza, F. & Viollier, R. D. 2002, ApJ, 564, 274
 Murphy, B.W., Cohn, H.N., Durisen, R.H., 1991, ApJ 370, 60
 Rauch, K. P. & Tremaine, S., 1996, 1996, New A, 1, 149R
 Reid, M. J., Menten, K. M., Genzel, R., Ott, T., Schödel, R. & Eckart, A., 2003, ApJ, 587, 208
 Reid, M. J. 1993, Annu. Rev. Astron. Astrophys., 31, 345
 Roberts D. A. & Goss W. M., 1993, ApJS, 317, 133
 Rubilar, G. F. & Eckart 2001, A., A&A, 374, 95
 Serabyn, E. & Lacy 1985, J. H., ApJ, 293, 445
 Spitzer, L. Jr. 1975, Dynamical Evolution of Globular Clusters, Princeton Series in Astrophysics
 Spurzem, R. 1999, J. Comp. Appl. Math, 109, 407
 Schödel, R., Ott, T., Genzel, R., Hofmann, R., Lehnert, M., Eckart, A., Mouawad, N., Alexander, T., Reid, M. J., Lenzen, R., Hartung, M., Lacombe, F., Rouan, D., Gendron, E., Rousset, G., Lagrange, A.-M., Brandner, W., Ageorges, N., Lidman, C., Moorwood, A. F. M., Spyromilio, J., Hubin, N., Menten, K. M. 2002,

Table A1. Orbital parameters of three exemplary 1σ fitting orbits.

				Min	Max
Total Mass M_{tot} ($10^6 M_{\odot}$)	3.65	4.10	4.80	3.28	5.40
Point Mass M_{BH} ($10^6 M_{\odot}$)	3.65	3.69	3.65	3.28	3.97
Cusp Percentage(%)	0.0	10	25	0	35
M^{apo} : Cusp mass inside S2's orbit($10^6 M_{\odot}$)	0.001	0.049	0.133	0	0.26
e : Eccentricity	0.88	0.882	0.881	0.868	0.897
i : Inclination($^{\circ}$)	-47.89	-47.88	-48.12	-46.86	-50.19
a : Semi-major axis(mpc)	4.65	4.66	4.59	4.52	4.79
T : Time of peri-centre passage	2002.327	2002.328	2002.333	2002.327	2002.337
Ω : Angle of line of nodes($^{\circ}$)	45.3	45.38	44.59	42.17	46.1
ω : Angle to peri-centre($^{\circ}$)	145.1	144.84	145.6	144.1	147.7
P : Period (Years)	15.55	15.43	15.06	14.61	16.67
Peri-Centre distance	0.557	0.552	0.55	0.511	0.6
$\Delta\alpha$: Peri-centre-shift per revolution	00°00'00"	00°40'48"	01°52'43"	00°00'00"	03°07'12"

Nature, 419, 694

Schödel, R., Ott, T., Genzel, R., Eckart, A., Mouawad, N., Alexander, T. 2003, ApJ, 596, 1015

Schödel, R., 2004, PHD Thesis, Ludwig-Maximilians-Universität, München

Zoccali, M., Renzini, A., Ortolani, S., Greggio, L., Saviane, I., Cas-sisi, S., Rejkuba, M., Barbuy, B., Rich, R. M., Bica, E., 2003, A&A, 399, 931Z